Handling Quality Improvements for the Flying-V Aircraft using Incremental Nonlinear Dynamic Inversion

van Overeem, S.; Wang, Xuerui; van Kampen, E.

DOI
10.2514/6.2023-0105

Publication date
2023

Document Version
Final published version

Published in
AIAA SciTech Forum 2023

AIAA SciTech Forum
23-27 January 2023, National Harbor, MD & Online
AIAA SCITECH 2023 Forum

10.2514/6.2023-0105

Handling Quality Improvements for the Flying-V Aircraft using Incremental Nonlinear Dynamic Inversion

Simon van Overeem*, Xuerui Wang†, and Erik-Jan van Kampen‡
Delft University of Technology, The Netherlands, 2629 HS Delft

Considerable growth in the number of passengers and cargo transported by air is predicted. Moreover, aircraft noise and climate impact become increasingly important factors in aircraft design. These existing challenges in aviation boost interest in the design of innovative aircraft configurations. One of these configurations is a V-shaped flying wing named the Flying-V. This work aims at developing a flight control system for the Flying-V that can be used to improve the stability and handling qualities of the aircraft. Prior work shows that the Flying-V is not able to adhere to all stability and handling quality requirements at the forward and aft centre of gravity location during cruise and approach. This paper illustrates how an Incremental Nonlinear Dynamic Inversion flight control system can be used to improve the stability and handling qualities of the aircraft. Furthermore, the robustness of the flight control system is assessed by analysing the effects of aerodynamic uncertainty on the attitude tracking error of the Flying-V. Upon implementation of the flight control system, this research shows that the eigenmodes become stable. Besides that, the flight control system is proved to be robust against aerodynamic uncertainty.

I. Introduction

Over the last fifty years, most commercial aircraft consisted of the traditional tube-and-wing configuration. This conventional design has obtained significant efficiency gains of 100% over the years [1]. However, the Airbus A350 and Boeing 787 represent an aircraft efficiency asymptote. Besides that, the number of passengers and cargo transported by air is predicted to grow considerably [2]. Furthermore, due to the increasing pressure on noise pollution and environmental impact, it is necessary to find a solution that is able to boost the efficiency of aircraft, while reducing noise and environmental impact [3]. One course of action to tackle the existing challenges in aviation is the design of an innovative aircraft configuration. The flying wing is one of the most promising aircraft configurations to overcome the existing challenges in aviation. The flying wing has different settings, such as the Blended-Wing-Body (BWB), C-Wing, and Tail-less aircraft. This type of aircraft has the potential to increase efficiency, resulting in less pollution. Furthermore, it is expected that noise levels during landing and take-off are reduced [3].

The Flying-V is a specific type of flying wing that is tailless, V-shaped, and consists of two cylindrical pressurised cabins located in the leading edge of the wing. The main advantage of the design of a Flying-V aircraft concept compared to conventional tube-and-wing aircraft is the reduction of wetted area and frictional drag. Namely, the Flying-V consists of one structure that integrates the structural function of accommodating payload and aerodynamic function of providing lift [4]. Furthermore, due to the smooth shape of this aircraft, it suffers less from interference drag. Additionally, the reduction of wetted area results in a reduced zero-lift drag [5]. This results in the fact that this type of aircraft can achieve a higher lift-to-drag ratio compared to conventional aircraft, meaning that it has a reduced fuel burn and takeoff weight [6, 7]. Research indicates that the aerodynamic efficiency gains of the Flying-V range between 10% and 25% compared to conventional tube-and-wing aircraft of similar size and weight. Additionally, the location of the engines on top of the wing reduces the noise level [2, 7]. The preliminary design of the Flying-V can be observed in Fig. 1.

Currently, the main Flying-V design challenge is centred on the improvement of the stability and handling qualities of this novel aircraft design for certification and qualification purposes. Previous research is conducted on the stability and handling qualities of the full-size aircraft by designing a six-degrees-of-freedom flight dynamic simulation model [8]. This flight dynamic simulation model makes use of an aerodynamic model that combines aerodynamic coefficients obtained from the Vortex Lattice Method with wind tunnel experiments. This combined aerodynamic model is able to capture the undesired behaviour of the Flying-V obtained from previous research, such as the unstable Dutch roll

*Graduate Student, Faculty of Aerospace Engineering at Delft University of Technology, s.vanovereem@student.tudelft.nl
†Assistant Professor, Faculty of Aerospace Engineering at Delft University of Technology, X.Wang-6@tudelft.nl, AIAA member
‡Assistant Professor, Faculty of Aerospace Engineering at Delft University of Technology, E.vanKampen@tudelft.nl

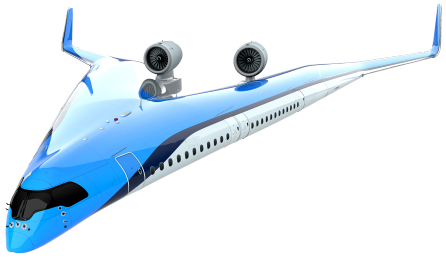

Fig. 1 The Flying-V aircraft.*

mode and longitudinally unstable behaviour [9–11]. The stability and handling qualities are assessed during cruise and approach conditions at the forward and aft centre of gravity locations obtained from previous research [9]. It is concluded that the Flying-V is not able to adhere to all stability and handling qualities during cruise and approach conditions at the forward and aft centre of gravity location. The stability and handling quality assessment are based on the trimmability of the Flying-V, the responses of the eigenmodes, and handling qualities such as the Control Anticipation Parameter (CAP). The analysis performed previously shows that during the approach at the forward centre of gravity location, the Flying-V meets the stability and handling qualities the least. At this flight condition, an elevon deflection of 20.2° is required to trim the aircraft. Due to an elevon deflection limit of 25°, this elevon trim deflection reduces the manoeuvrability of the Flying-V. Besides that, the phugoid mode and Dutch roll mode are unstable [8]. To improve the stability and handling qualities of the Flying-V, there is a necessity to design a flight control system. This flight control system is required to cope with the inherent nonlinear behaviour of the aerodynamic model used for the flight dynamic simulation. Furthermore, due to the assumptions made during the design of the flight dynamic simulation model and the uncertainties present in the aerodynamic model, the flight control system has to cope with these model uncertainties to diminish performance degradation [8].

A couple of decades ago, almost all flight control systems for aircraft were designed using classical (linear) control techniques [12]. Even though the systems involved with aircraft control are nonlinear, it is still possible to apply a linear controller to this system by making the key assumption that the linear controller is only applied to a small range within the complete flight envelope [13]. This requires the design of multiple linear controllers to cover the complete flight envelope and construct a gain schedule by interpolating the gains with respect to the flight condition. This procedure is very time consuming, expensive, and is not flexible regarding design changes [14]. Furthermore, during the design of a linear controller, it is necessary to assume that the parameters of the aircraft model are well known, which is not the case for the Flying-V. Therefore, it may exhibit performance degradation or instability [13]. To overcome the shortcomings of linear controllers, several nonlinear control methods have emerged over the past years. One of these nonlinear control methods is known as Incremental Nonlinear Dynamic Inversion (INDI). INDI is a sensor-based control method that requires less model information and can therefore improve the system robustness against model uncertainties [15]. This is especially useful for the control system design of the Flying-V due to the assumptions and uncertainties present in the flight dynamic simulation model. The INDI control has also be further developed into incremental backstepping control [16] and incremental sliding mode control [17].

The contribution of this study to research related to the Flying-V consists of the design of an Incremental Nonlinear Dynamic Inversion (INDI) controller to improve the stability and handling qualities of the Flying-V during approach at the forward centre of gravity location. This flight condition is selected due to the unfavourable stability and handling qualities obtained from previous research [8]. The controller is assessed by first analysing the stability and handling qualities of the controlled aircraft. After that, the robustness of the controller is assessed by analysing the effects of aerodynamic uncertainty on the attitude tracking error of the Flying-V aiming to follow a reference trajectory.

The rest of this paper is structured as follows. Section II elaborates on the Flying-V flight dynamic simulation model and the essential stability and handling qualities obtained from previous research. Besides that, the flight control system design and robustness analysis methodology are discussed. Section III, discusses the stability and handling qualities of the controlled Flying-V and shows the robustness of the flight control system. Finally, conclusions are discussed in section IV and recommendations for further research are given in section V.

II. Methodology

In this section, the methodology to design an Incremental Nonlinear Dynamic Inversion (INDI) flight control system is discussed. First of all, section II.A elaborates on the layout of the Flying-V. Secondly, section II.B talks about the dynamic simulation model used for the flight control system design. Furthermore, section II.C shows the essential stability and handling qualities of the Flying-V. Besides that, section II.D develops the methodology for the flight control system design. After that, the robustness assessment is discussed in section II.E. Finally, section II.F elaborates on the assumptions and limitations of the controller design.

A. Flying-V Layout

In Fig. 2* it is possible to observe the general layout of the Flying-V used for the analysis in this research. The figure shows the V-shaped wing planform with engines mounted on top of the aircraft. These engines can be used to control the airspeed. Besides that, the Flying-V consists of a set of inboard elevons (CS1) and outboard elevons (CS2) mounted on each side of the wing. Both elevons can be used for pitch control, whereas only the outboard elevons are used for roll control. Furthermore, due to the tailless design of the aircraft, the rudders (CS3) are integrated into the winglets and can be used for yaw control. The forward centre of gravity is located 29.4 m from the nose of the aircraft. The aft centre of gravity is located 31.7 m from the nose of the aircraft.

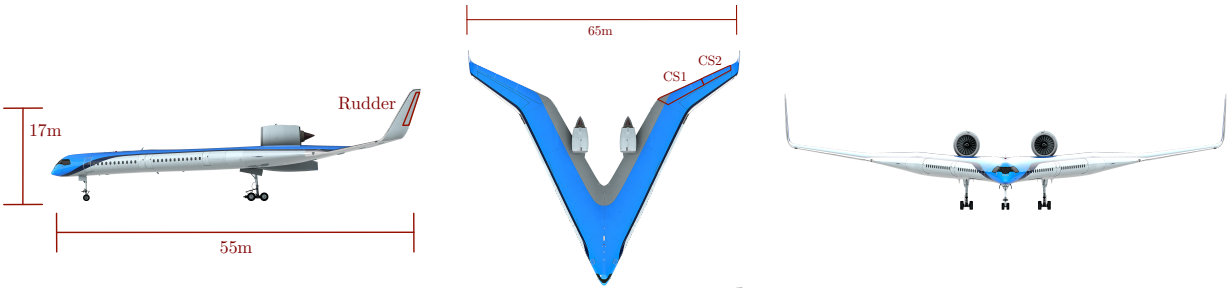

Fig. 2 Flying-V layout.*

B. Flight Dynamic Simulation Model

To develop a flight control system that is able to improve the stability and handling qualities of the Flying-V, a six degrees-of-freedom flight dynamic simulation model is used. The development of this simulation model is discussed in [8]. The simulation model can be used for the cruise condition and approach condition for several centre of gravity locations. Besides that, to estimate the components of the inertia matrix, the lumped mass method is used [8].

Previous research dictates that the undesired behaviour of the Flying-V consists of an unstable Dutch roll mode and longitudinal instability for angles of attack larger than 20°. The unstable Dutch roll is obtained from a stability and handling quality analysis using aerodynamic coefficients obtained from the Vortex Lattice Method [9]. Besides that, the longitudinal unstable behaviour of the aircraft was observed during wind tunnel experiments [11, 18] and captured in an aerodynamic model obtained from these wind tunnel experiments [10]. These aerodynamic models are combined into a single aerodynamic model that is able to capture both the unstable Dutch roll and longitudinal instability for angles of attack larger than 20° for the full-scale aircraft.

C. Stability and Handling Quality analysis

In this subsection, the stability and handling qualities of the Flying-V are discussed. In section II.C.1 the location of the eigenvalues are shown. After that, section II.C.2 shows an assessment of the eigenmodes by comparing the eigenmodes with military standards. Finally, section II.C.3 elaborates on the handling qualities of the Flying-V by analysing the Control Anticipation Parameter.

*https://www.tudelft.nl/lr/flying-v

1. Eigenvalue Analysis

Table 1 shows the eigenvalues obtained from the linearised equations of motion during approach at the forward centre of gravity location [8]. Besides that, the damping ratio and natural frequency of the modes are displayed. This specific flight condition is considered the worst flight condition due to the large elevon deflection required to trim the Flying-V and undesired eigenmodes. Namely, from the eigenvalues shown in Table 1 it can directly be deduced that the phugoid mode and Dutch roll mode are unstable. Also, the spiral mode is unstable, but as is discussed in Section II.C.2 this mode is able to adhere to military standards.

Table 1 Eigenvalues at forward centre of gravity location during approach [8].

Eigenmode	Eigenvalue	Damping Ratio	Natural Frequency
Short Period	$-0.47 \pm 0.50i$	0.683	0.681
Phugoid	$4.0 \cdot 10^{-4} \pm 0.16$	$-2.31 \cdot 10^{-3}$	0.161
Dutch roll	$8.1 \cdot 10^{-2} \pm 0.99i$	$-8.14 \cdot 10^{-2}$	0.992
Aperiodic Roll	-0.79	-	-
Spiral	$2.04 \cdot 10^{-2}$	-	-

2. Modes Response Analysis

The flying quality analysis performed for the Flying-V at the forward centre of gravity location during approach is summarised in Table 2 [8, 19]. This table shows that the short period mode had level 1 flying qualities. Besides that, the phugoid mode and Dutch roll mode cannot be rated using these requirements due to the short (unstable) period of the phugoid mode and unstable behaviour of the Dutch roll mode. Finally, the aperiodic roll mode and spiral mode show level 1 flying qualities.

Table 2 Flying-V flying qualities during approach at forward centre of gravity location [8, 19].

Eigenmode	**Values Flying-V**	**Requirements**
Short Period	$\varsigma_{sp} = 6.83 \cdot 10^{-1}$	Level 1: $0.5 < \varsigma_{sp} < 1.3$
		Level 2: $0.35 < \varsigma_{sp} < 2.0$
		Level 3: $\varsigma_{sp} > 0.25$
Phugoid	Unstable but $T_{ph} = 39.0s$	Level 1: $\varsigma_{ph} > 0.04$
		Level 2: $\varsigma_{ph} > 0$
		Level 3: Unstable but $T_{ph} > 55s$
Dutch roll	Unstable	Level 1: $\varsigma_d > 0.08$ $\varsigma_d\omega_d > 0.10$ $\omega_d > 0.5$
		Level 2: $\varsigma_d > 0.02$ $\varsigma_d\omega_d > 0.05$ $\omega_d > 0.5$
		Level 3: $\varsigma_d > 0$ $\omega_d > 0.4$
Aperiodic Roll	$T_r = 1.26s$	Level 1: $T_r < 1.4s$
		Level 2: $T_r < 3.0s$
		Level 3: $T_r < 10.0s$
Spiral	$T_s = 42.6s$	Level 1: $T_s > 17.3s$
		Level 2: $T_s > 11.5s$
		Level 3: $T_s > 7.2s$

3. Handling Quality Analysis

The handling qualities of an aircraft are considered as a description of the adequacy of the short term dynamic response to controls during the execution of a flight task [20]. The handling qualities discussed in this research involve

quantitative handling qualities as these quantitative methods do not require pilot-in-the-loop experiments. The handling quality assessed for this research is the Control Anticipation Parameter (CAP). This is a measure of the manoeuvrability of the aircraft. In case the CAP is too high, the aircraft's response is faster than would be expected by the pilot resulting in understeering. On the other hand, in case the CAP is too low, the aircraft's response is sluggish, which results in oversteering [9]. The Control Anticipation Parameter is equal to 0.16 at the forward centre of gravity location during approach. This is also shown in Fig. 3, where it can be observed that the CAP is at the border of the Level 1 handling qualities region [8].

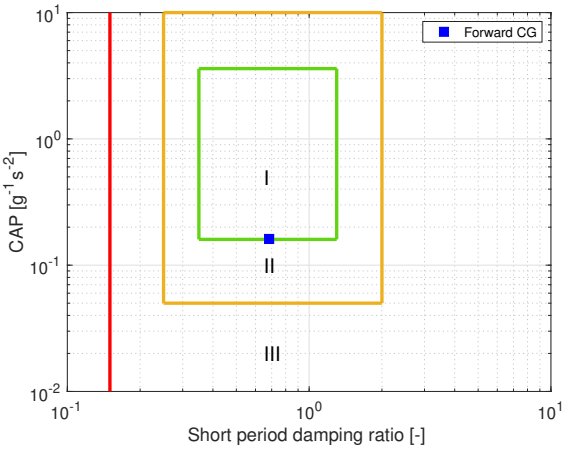

Fig. 3 Control Anticipation Parameter at forward centre of gravity location during cruise [8].

D. INDI Flight Control System Design

In this subsection, the design of the INDI flight control system is discussed. First of all, the INDI derivation is shown in section II.D.1. After that, section II.D.2 elaborates the inner-loop stability augmentation system design. Finally, the outer-loop control augmentation system design is discussed in section II.D.3.

1. INDI Derivation

Incremental Nonlinear Dynamic Inversion (INDI) is a sensor based control method which is derived using an incremental dynamic equation. INDI has reduced model dependency than Nonlinear Dynamic Inversion (NDI) and therefore has an improved robustness of the closed-loop system compared to an NDI controller [21]. One of the differences between an NDI controlled system and INDI controlled system originates from the control input. The NDI controller provides a complete command control input, whereas an INDI controller considers the influence of increments of control commands in the dynamics. These increments in the control commands are provided as a function of the error of the controlled variables [22]. To derive the equations for an INDI controller, it is possible to start with the general equation for a nonlinear system shown in Eq. (1).

$$\dot{\boldsymbol{x}} = \boldsymbol{f}(\boldsymbol{x}, \boldsymbol{u}) \tag{1}$$

Taking the Taylor series expansion of this equation at the current time point, it is possible to linearise the system as shown in Eq. (2).

$$\begin{aligned} \dot{\boldsymbol{x}} &= \boldsymbol{f}(\boldsymbol{x}_0, \boldsymbol{u}_0) + \left.\frac{\partial \boldsymbol{f}(\boldsymbol{x}, \boldsymbol{u})}{\partial \boldsymbol{x}}\right|_{\boldsymbol{x}=\boldsymbol{x}_0, \boldsymbol{u}=\boldsymbol{u}_0} (\boldsymbol{x} - \boldsymbol{x}_0) + \left.\frac{\partial \boldsymbol{f}(\boldsymbol{x}, \boldsymbol{u})}{\partial \boldsymbol{u}}\right|_{\boldsymbol{x}=\boldsymbol{x}_0, \boldsymbol{u}=\boldsymbol{u}_0} (\boldsymbol{u} - \boldsymbol{u}_0) + O(\Delta \boldsymbol{x}^2, \Delta \boldsymbol{u}^2) \\ &= \dot{\boldsymbol{x}}_0 + \boldsymbol{G}(\boldsymbol{x}_0, \boldsymbol{u}_0)(\boldsymbol{u} - \boldsymbol{u}_0) + \boldsymbol{\delta} \end{aligned} \tag{2}$$

Under sufficiently high sampling frequency, the INDI control input is designed as [15]

$$\Delta \boldsymbol{u} = \boldsymbol{G}^{-1}(\boldsymbol{x}_0, \boldsymbol{u}_0)(\boldsymbol{\nu} - \dot{\boldsymbol{x}}_0) \tag{3}$$

where $\boldsymbol{\nu}$ is the virtual control input. This control law results in increments of the control commands, meaning that these changes must be added to the current reference command in order to obtain the full new control command input. This means that the total control command can be obtained using Eq. (4).

$$\boldsymbol{u} = \boldsymbol{u}_0 + \Delta\boldsymbol{u} = \boldsymbol{u}_0 + \boldsymbol{G}^{-1}(\boldsymbol{x}_0, \boldsymbol{u}_0)(\boldsymbol{\nu} - \dot{\boldsymbol{x}}_0) \tag{4}$$

In Eq. (4) it can be observed that the INDI controller does not depend on the exact knowledge of the system dynamics ($\boldsymbol{f}(\boldsymbol{x})$). Instead, the control strategy is merely dependent on the sensor measurements of the time derivative of the state ($\dot{\boldsymbol{x}}_0$) and actuator dynamics measurements ($\boldsymbol{u}_0$). Therefore, the dependency of the closed-loop system has decreased resulting in improved performance in case of model mismatch and model uncertainties. However, it needs to be noted that this controller is not completely independent of the model as changes in the system dynamics are reflected in the derivative of the state vector ($\dot{\boldsymbol{x}}_0$). On the other side, the performance of this controller is expected to be more sensitive to sensor aspects such as noise, bias, and misalignments than an NDI controller [22]. The layout of the closed-loop system including an INDI controller is shown in Fig. 4.

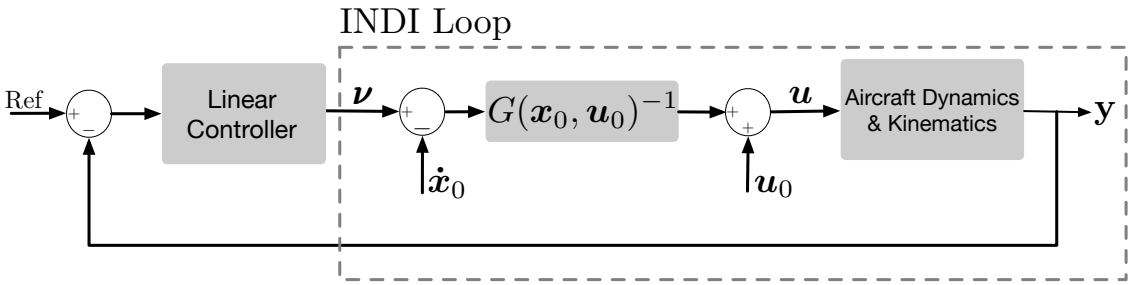

Fig. 4 Block diagram for INDI controller.

2. Stability Augmentation System Design

The stability augmentation system consists of an INDI controller used to control the angular rates and a Proportional-Integral-Derivative (PID) controller to control the airspeed. Due to the slow engine dynamics, it is not possible to control the airspeed using INDI. Therefore, it is decided to use a PID controller to control the airspeed. The angular rate loop is based on the rotational equations of motion as shown in Eq. (5). In this equation, $\boldsymbol{\omega}$ represents the angular rates, $\boldsymbol{J}$ is the inertia matrix, and $\boldsymbol{M}$ represents the moment vector acting on the Flying-V.

$$\dot{\boldsymbol{\omega}} = \boldsymbol{J}^{-1}\boldsymbol{M} - \boldsymbol{J}^{-1}(\boldsymbol{\omega} \times \boldsymbol{J}\boldsymbol{\omega}) \tag{5}$$

Consequently, to obtain the matrix $\boldsymbol{G}(\boldsymbol{x}_0, \boldsymbol{u}_0)$ shown in Eq. (2), it is necessary to differentiate the nonlinear differential equation with respect to the inputs (δ_{CS1}, δ_{CS2}, and δ_{CS3}). After that, the control surface inputs can be calculated. This results in Eq. (6) and Eq. (7), respectively. In Eq. (6) it can be observed that the inboard elevons (δ_{CS1}) are only used for pitch control. Besides that, the outboard elevons (δ_{CS2}) are used for roll-, pitch-, and yaw control. Furthermore, the control surfaces attached to the winglets (δ_{CS3}) are used for roll- and yaw control. Also, ρ is the atmospheric density, V is the total airspeed (which can also be represented as $V = \sqrt{u^2 + v^2 + w^2}$), S is the wing surface area, and $\bar{c}$ is the mean aerodynamic chord. The block diagram of the stability augmentation system is shown in Fig. 5. The actuator dynamics and engine dynamics are modelled using a first-order lag system with a bandwidth of 35.2 rad/s [23] and 5.0 rad/s respectively [24]. Besides that, the saturation values correspond to [-25°, 25°] for the control surfaces [10] and [0 N, $3.79{\cdot}10^5$ N] for the engines [25]. The gains of the stability augmentation system are tuned manually. The gains are tuned by first increasing the proportional gain such that the Flying-V is able to track a reference angular rate or airspeed. After that, the oscillations are removed by increasing the derivative gain. In case any steady state error is present, this is removed using the integral gain. The gains of the stability augmentation system are shown in Table 3.

$$\boldsymbol{G}_{\omega}(\boldsymbol{x}_0, \boldsymbol{u}_0) = \boldsymbol{J}^{-1}\frac{1}{2}\rho V^2 S\bar{c}\begin{bmatrix} C_{l_{\delta_{\text{CS1}}}} & C_{l_{\delta_{\text{CS2}}}} & C_{l_{\delta_{\text{CS3}}}} \\ C_{m_{\delta_{\text{CS1}}}} & C_{m_{\delta_{\text{CS2}}}} & C_{m_{\delta_{\text{CS3}}}} \\ C_{n_{\delta_{\text{CS1}}}} & C_{n_{\delta_{\text{CS2}}}} & C_{n_{\delta_{\text{CS3}}}} \end{bmatrix} = \boldsymbol{J}^{-1}\frac{1}{2}\rho V^2 S\bar{c}\begin{bmatrix} 0 & C_{l_{\delta_{\text{CS2}}}} & C_{l_{\delta_{\text{CS3}}}} \\ C_{m_{\delta_{\text{CS1}}}} & C_{m_{\delta_{\text{CS2}}}} & 0 \\ 0 & C_{n_{\delta_{\text{CS2}}}} & C_{n_{\delta_{\text{CS3}}}} \end{bmatrix} \tag{6}$$

$$\boldsymbol{u} = \boldsymbol{u}_0 + \frac{2\boldsymbol{J}}{\rho V^2 S\bar{c}} \begin{bmatrix} 0 & C_{l_{\delta_{CS2}}} & C_{l_{\delta_{CS3}}} \\ C_{m_{\delta_{CS1}}} & C_{m_{\delta_{CS2}}} & 0 \\ 0 & C_{n_{\delta_{CS2}}} & C_{n_{\delta_{CS3}}} \end{bmatrix}^{-1} (\boldsymbol{\nu} - \dot{\boldsymbol{\omega}}) \tag{7}$$

$$\boldsymbol{u} = \begin{bmatrix} \delta_{CS1} \\ \delta_{CS2} \\ \delta_{CS3} \end{bmatrix}; \quad \boldsymbol{\nu} = \begin{bmatrix} \nu_p \\ \nu_q \\ \nu_r \end{bmatrix}; \quad \boldsymbol{\omega} = \begin{bmatrix} p \\ q \\ r \end{bmatrix}$$

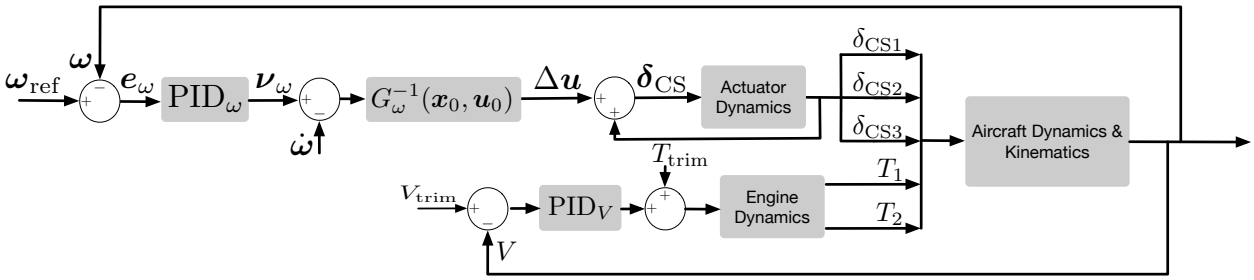

Fig. 5 INDI controller inner-loops.

3. Control Augmentation System Design

The control augmentation outer-loop consists of the control of the roll angle, flight path angle, and sideslip angle. The choice for controlling these variables is obtained from the Airbus A350-900 aircraft, which is used as a reference aircraft for the design of the Flying-V [2, 26]. Besides that, the flight path angle controller can be used to maintain the required flight path angle during approach [8, 19], and keeping the sideslip angle at zero results in coordinated flight [27]. The time-scale separation principle is used to obtain the control augmentation loop around the stability augmentation inner-loops. The principle of time-scale separation implies the use of several loops within the controller to take into account the fast dynamics and slow dynamics of the system. A variable is said to have slow dynamics in case the control effectiveness on the dynamics is low. In case a variable is said to have fast dynamics, the control effectiveness on the dynamics is high. This leads to a control system where the outputs of the slow outer-loop are used as a reference for the fast inner-loop [27].

The relation between the attitude angles and angular rates depends on the kinematic relation shown in Eq. (8). Because there is no model uncertainty nor error in the kinematic equations, this loop is based on Nonlinear Dynamic Inversion (NDI) instead of INDI [23].

$$\underbrace{\begin{bmatrix} \dot{\phi} \\ \dot{\theta} \end{bmatrix}}_{\begin{bmatrix} \nu_\phi & \nu_\theta \end{bmatrix}^T} = \underbrace{\begin{bmatrix} 1 & \sin\phi\tan\theta & \cos\phi\tan\theta \\ 0 & \cos\phi & -\sin\phi \end{bmatrix}}_{\begin{bmatrix} a_\phi(\boldsymbol{x}) & a_\theta(\boldsymbol{x}) \end{bmatrix}^T} \begin{bmatrix} p \\ q \\ r \end{bmatrix} \tag{8}$$

The sideslip dynamic inversion loop can be used to compensate the sideslip angle to perform coordinated turns, whereas the roll angle and flight path angle can be controlled. The sideslip angle can be computed as is shown in Eq. (9). In this equation, β represents the sideslip angle and v is the lateral body velocity component.

$$\beta = \arcsin\frac{v}{V} \tag{9}$$

Taking the derivative of the sideslip angle with respect to time results in Eq. (10). This equation can be rewritten as Eq. (11).

$$\dot{\beta} = \frac{\dot{v}V - v\dot{V}}{V\sqrt{u^2+w^2}} = \frac{\dot{v}}{\sqrt{u^2+w^2}} - \frac{v(u\dot{u} + v\dot{v} + w\dot{w})}{(u^2+v^2+w^2)\sqrt{u^2+w^2}} \tag{10}$$

$$\underbrace{\dot{\beta}}_{\nu_\beta} = \underbrace{\left(\frac{1}{\sqrt{u^2+w^2}}\right)\left(A_x + A_y + A_z\right)}_{b_\beta(\boldsymbol{x})} + \underbrace{\begin{bmatrix} \frac{w}{\sqrt{u^2+w^2}} & 0 & \frac{-u}{\sqrt{u^2+w^2}} \end{bmatrix}}_{a_\beta(\boldsymbol{x})} \begin{bmatrix} p \\ q \\ r \end{bmatrix} \tag{11}$$

$$A_x = \frac{uv}{V^2}\left(\frac{F_x}{m} - g\sin\theta\right)$$
$$A_y = \left(1 - \frac{v^2}{V^2}\right)\left(\frac{F_y}{m} + g\sin\phi\cos\theta\right)$$
$$A_z = -\frac{vw}{V^2}\left(\frac{F_z}{m} + g\cos\phi\cos\theta\right)$$

Combining Eq. (8) and Eq. (11) results in Eq. (12). To control the flight path angle, another control loop is added to the system including a PID controller that is used for flight path angle control. The gains for the control augmentation system are tuned similarly to the stability augmentation system and are shown in Table 3. Besides that, the block diagram of the control augmentation loop is shown in Fig. 6.

$$\boldsymbol{\omega}_{\text{ref}} = \begin{bmatrix} a_\phi(\boldsymbol{x}) \\ a_\theta(\boldsymbol{x}) \\ a_\beta(\boldsymbol{x}) \end{bmatrix}^{-1} \left(\begin{bmatrix} \nu_\phi \\ \nu_\theta \\ \nu_\beta \end{bmatrix} - \begin{bmatrix} 0 \\ 0 \\ b_\beta(\boldsymbol{x}) \end{bmatrix} \right) \tag{12}$$

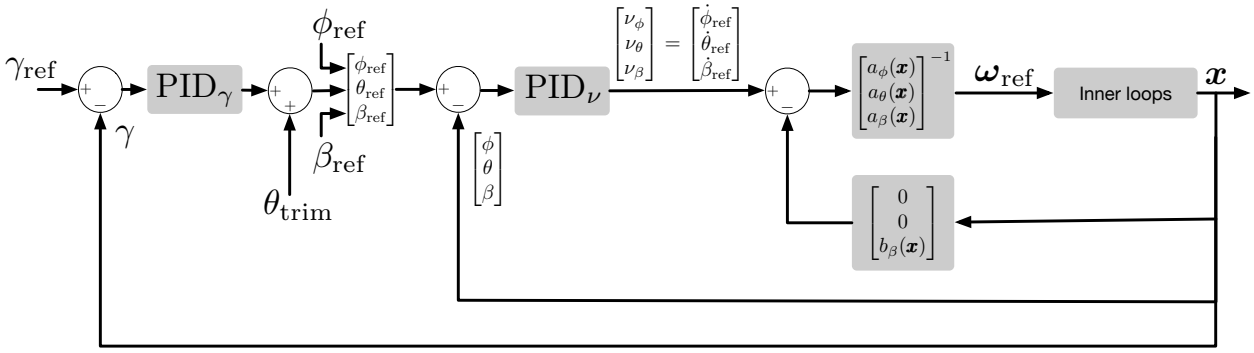

Fig. 6 INDI guidance control loops.

Table 3 Controller gains for flight control system.

	PID_ω			PID_V	PID_ν			PID_γ
	p	q	r		ϕ	θ	β	
K_p	1	1	2	50000	1	1	1	1
K_i	0.1	0	0	0	0	0	0	0.2
K_d	0	0	0	30000	1	2	0	0.02

E. Robustness Analysis

Due to the assumptions made during the construction of the aerodynamic model and the inherent uncertainties present in the aerodynamic coefficients obtained from the Vortex Lattice Method and wind tunnel experiments, one of the main components of uncertainty in the simulation model is the aerodynamic model [8]. Referring to the Lyapunov-based stability and robustness analysis in [15], when the sampling frequency is sufficiently high, the INDI control is robust to the term $\boldsymbol{\delta}$ in Eq. (2). Also, it can passively tolerate a certain range of uncertainties in $\boldsymbol{G}(\boldsymbol{x})$.

To apply aerodynamic uncertainty to the aerodynamic coefficients, Eq. (14) is used. In this equation, $C_*(\Delta)$ represents one of the sub-coefficients, whereas $\hat{C}_*(\Delta)$ represents the sub-coefficient subjected to aerodynamic uncertainty. Besides that, n represents the scaling factor and $N(0,1)$ represents a normal distribution with a mean equal to zero and a standard deviation equal to one. Previous research dictates a maximum error of 25% during the validation process of the aerodynamic coefficients obtained from the Vortex Lattice Method by comparing these coefficients to aerodynamic coefficients obtained from wind tunnel experiments [9]. Therefore, it is decided to vary the scaling factor in the following range: $\begin{bmatrix} 0.0 & 0.05 & 0.10 & 0.15 & 0.20 & 0.25 \end{bmatrix}$. The result of this methodology is that aerodynamic uncertainty is applied to each aerodynamic sub-coefficient by adding a normal distribution to the coefficient with a mean equal to zero and standard deviation ranging between 0% and 25% of $C_*(\Delta)$.

$$C_* = C_*(\alpha) + C_*(\alpha,\beta) + C_*(\alpha,p) + C_*(\alpha,q) + C_*(\alpha,r) + C_*(\alpha,\delta_{CS1}) + C_*(\alpha,\delta_{CS2}) + C_*(\alpha,\delta_{CS3}) \tag{13}$$

$$\hat{C}_*(\Delta) = C_*(\Delta)(1 + nN(0,1)) \tag{14}$$

To analyse the robustness of the flight control system, a reference trajectory is designed for the flight path angle controller and roll angle controller, while maintaining coordinated flight ($\beta_{ref} = 0$). It is decided to design a 3211 manoeuvre for the flight path angle and roll angle reference trajectory. The magnitude of the 3211 manoeuvre is selected such that actuator saturation is taken into account. Namely, increasing the flight path angle or roll angle demand would result in higher actuator demands than possible due to saturation. The reference trajectories together with the nominal response of the INDI controlled Flying-V are displayed in Fig. 7. Besides that, the control surface deflections are shown in Fig. 8. Consequently, the Root-Mean-Squared Error (RMSE) is determined according to Eq. (15). In this equation, N represents the total number of timesteps during a simulation run, x_{ref} is the reference state, and x represents the actual state.

$$\text{RMSE} = \sqrt{\frac{1}{N}\sum_{i=0}^{N}(x_{ref_i} - x_i)^2} \tag{15}$$

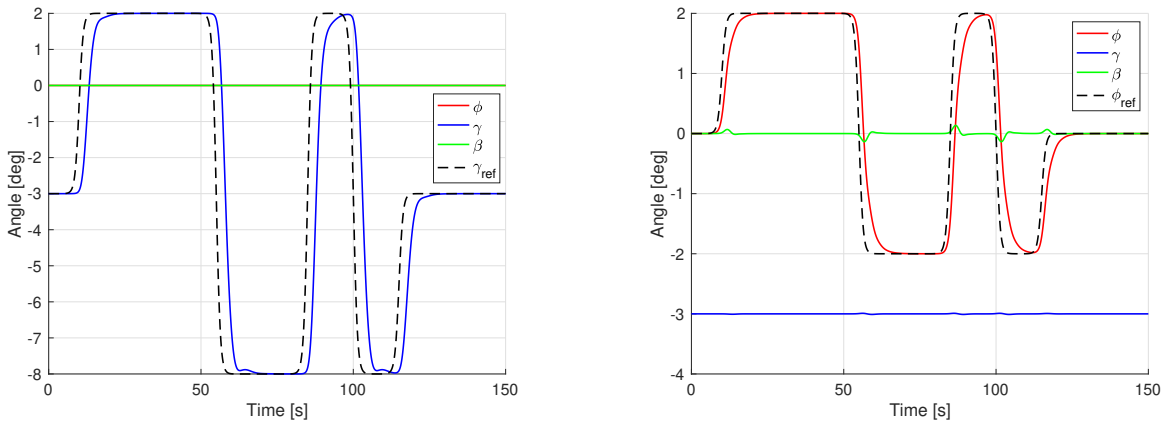

(a) Flight path angle reference trajectory and response.

(b) Roll angle reference trajectory and response.

Fig. 7 Reference trajectories and Flying-V response for flight path angle and roll angle.

F. Assumptions and Limitations

During the design and assessment of the flight control system, several assumptions and therefore accompanying limitations have to be taken into account.

First of all, during the design of the control system, no sensor dynamics are taken into account. This means that the measurements obtained from the sensors are readily available. Besides that, the measurements are not contaminated

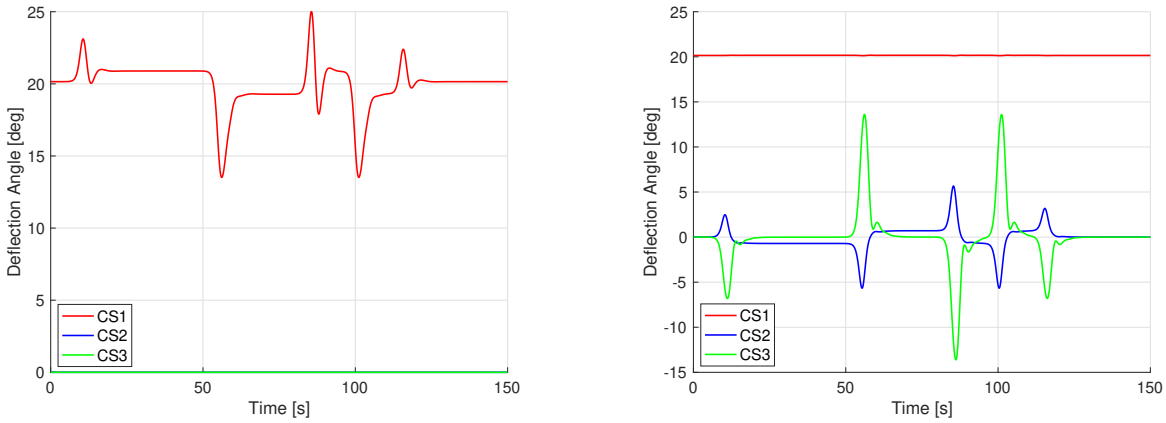

(a) Control surface deflections for flight path angle trajectory.

(b) Control surface deflections for roll angle trajectory.

Fig. 8 Control surface deflections for flight path angle and roll angle.

with noise and are not biased. The stability of INDI controllers subjected to measurement time delay is an issue. Especially, in case the actuator measurements and the state derivative measurements are not equally delayed. Introducing measurement time delay to the system results in a reduced stability region for the INDI controlled system [27].

Additionally, it is assumed that the Flying-V experiences a perfect atmosphere that corresponds to the International Standard Atmosphere without any turbulence. In reality, the Flying-V is likely to experience turbulence. Adding turbulence to the system deteriorates the tracking response of the Flying-V. Therefore, additional turbulence increases the RMSE of the tracking task [15].

Finally, when determining the robustness of the INDI controller to aerodynamic uncertainty, previous research dictates a maximum error of 25% between aerodynamic coefficients obtained from the Vortex Lattice Method and wind tunnel experiments [8, 9]. To compare these aerodynamic models it is necessary to assume that the relative density factor and the relative moment of inertia of both models are equal. Because these parameters are different, the actual maximum error between both aerodynamic models likely deviates from the value used in this research.

III. Results

In this section, the results obtained from the stability and handling quality analysis, and robustness assessment of the INDI controlled Flying-V are discussed. Section III.A discusses the stability and handling quality results. Besides that, the robustness results are shown in Section III.B.

A. Stability and Handling Quality Results

In this section, the stability and handling quality results are discussed. In Section III.A.1, the results from the eigenvalue analysis are shown and in Section III.A.2 the handling qualities are discussed.

1. Eigenvalue Results

As discussed in Section II.C, during approach at the forward centre of gravity location, the phugoid mode and Dutch roll mode of the Flying-V are unstable. To stabilise these modes, a stability augmentation system is applied to the aircraft as discussed in Section II.D.2. This section analyses how the eigenmodes of the Flying-V are affected by the application of the phugoid damper and yaw damper to the aircraft. In Fig. 9, the location of the eigenvalues for the uncontrolled and controlled system are displayed. These figures show that application of the stability augmentation system results in a stabilised phugoid mode and Dutch roll mode.

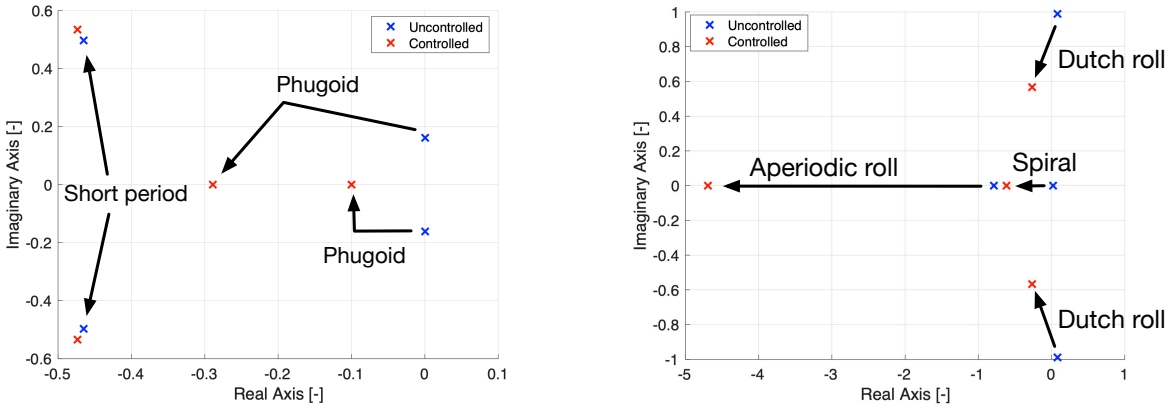

(a) Longitudinal Eigenvalues

(b) Lateral-directional Eigenvalues.

Fig. 9 Eigenvalue shift due to phugoid- and yaw dampers.

2. Modes Response Results

Besides that, the handling qualities of the controlled Flying-V are compared to military standards as shown in Table 4. In this table, the flying quality level of the controlled Flying-V is bold. This table shows that the damping ratio of the short period is equal to $\varsigma_{\text{sp}} = 6.63 \cdot 10^{-1}$, resulting in Level 1 handling qualities. Besides that, due to the phugoid damper, the phugoid mode is real and therefore has a damping ratio equal to $\varsigma_{\text{ph}} = 1.0$, resulting in Level 1 handling qualities. Furthermore, the application of the yaw damper stabilises the Dutch roll mode resulting in a damping ratio and natural frequency of $\varsigma_d = 0.42$ and $\omega_d = 0.57$ rad/s. Therefore, the Dutch roll mode is also rated Level 1. Also, the aperiodic roll mode has a characteristic time constant equal to $T_r = 0.21s$, indicating that this mode is rated Level 1. Finally, because the spiral mode is stable, it is rated Level 1.

Table 4 Flying-V flying qualities including a phugoid damper and yaw damper [19].

Eigenmode	Values Flying-V	Requirements		
Short Period	$\varsigma_{\text{sp}} = 6.63 \cdot 10^{-1}$	**Level 1:**	$\mathbf{0.5 < \varsigma_{sp} < 1.3}$	
		Level 2:	$0.35 < \varsigma_{\text{sp}} < 2.0$	
		Level 3:	$\varsigma_{\text{sp}} > 0.25$	
Phugoid	$\varsigma_{\text{ph}} = 1.0$	**Level 1:**	$\mathbf{\varsigma_{ph} > 0.04}$	
		Level 2:	$\varsigma_{\text{ph}} > 0$	
		Level 3:	Unstable but $T_{\text{ph}} > 55s$	
Dutch roll	$\varsigma_d = 0.42$ and $\omega_d = 0.57$ rad/s	**Level 1:**	$\mathbf{\varsigma_d > 0.08}$	$\mathbf{\varsigma_d \omega_d > 0.10}$ $\mathbf{\omega_d > 0.5}$
		Level 2:	$\varsigma_d > 0.02$	$\varsigma_d \omega_d > 0.05$ $\omega_d > 0.5$
		Level 3:	$\varsigma_d > 0$	$\omega_d > 0.4$
Aperiodic Roll	$T_r = 0.21s$	**Level 1:**	$\mathbf{T_r < 1.4s}$	
		Level 2:	$T_r < 3.0s$	
		Level 3:	$T_r < 10.0s$	
Spiral	Stable	**Level 1:**	$\mathbf{T_s > 17.3s}$	
		Level 2:	$T_s > 11.5s$	
		Level 3:	$T_s > 7.2s$	

B. Robustness Results

As discussed in section II.E, the robustness of the flight control system is determined by applying aerodynamic uncertainty to each aerodynamic coefficient. The aerodynamic uncertainty is determined by adding a normal distribution to each aerodynamic coefficient with a mean equal to zero and standard deviation ranging between 0% and 25% of the value of each aerodynamic coefficient. Consequently, 100 runs are performed for each standard deviation. This results in the boxplots shown in Fig. 10 and Fig. 11 for the flight path angle trajectory and roll angle trajectory respectively.

1. Flight Path Angle Robustness

In Fig. 10 the results of the robustness analysis applied to the flight path angle trajectory are shown. Fig. 10a presents the complete boxplots for the flight path angle trajectory, whereas Fig. 10b has zoomed in on the boxplots. In these figures, the RMSE is displayed for each n-factor as discussed in Eq. (14), ranging from 0 to 0.25. Looking at Fig. 10a it is possible to observe an increasing number of outliers with increasing n-factor. These outliers originate from the deflection limits of the control surfaces. In case the effectiveness of the control surfaces is reduced, a larger deflection is required to obtain the same pitch rate demand. However, the control surface deflection limit is equal to 25 degrees. This means that in case the control surface deflection demand is larger than 25 degrees, this control surface deflection demand cannot be achieved, resulting in a larger RMSE. Besides that, Fig. 10b shows that the upper and lower limit of each boxplot tends to increase with increasing aerodynamic uncertainty, while the median remains similar. Even though the upper limit of the boxplot increases, it needs to be noted that the RMSE is still within the same order of magnitude as the nominal case. This indicates that the INDI controller is barely affected by the aerodynamic uncertainty applied to the aerodynamic coefficients.

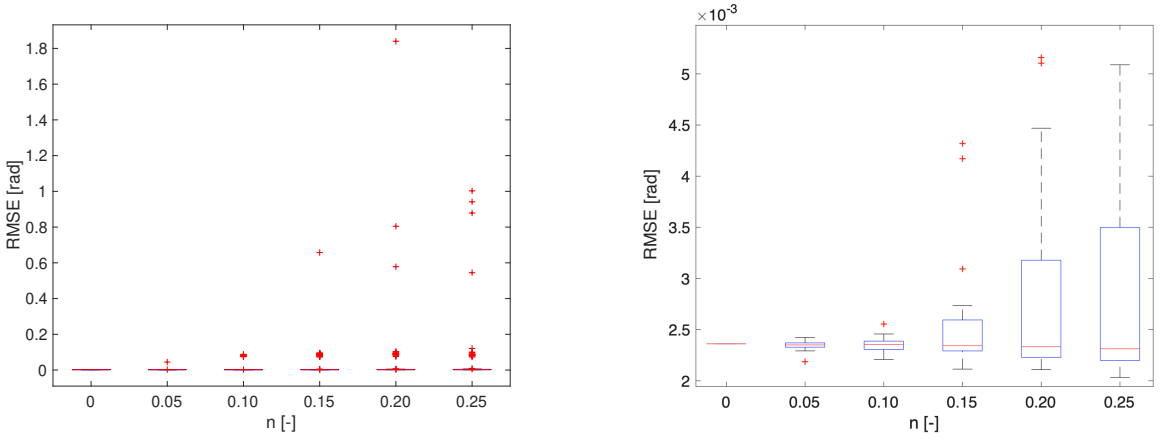

(a) Boxplot for flight path angle trajectory.

(b) Zoomed boxplot flight path angle.

Fig. 10 Boxplots showing flight path angle tracking error for aerodynamic uncertainty.

2. Roll Angle Robustness

In Fig. 11, the results of the robustness applied to the roll angle trajectory are shown. Fig. 11a presents the complete boxplots for the roll angle trajectory, whereas Fig. 11b has zoomed in on the boxplots. Also in these figures, the RMSE is displayed for each n-factor as discussed in Eq. (14), ranging from 0 to 0.25. Also in Fig. 11a it is possible to observe several outliers, indicating that these outliers are the results of elevon deflection demands that could not be met. Besides that, Fig. 11b shows similar results as Fig. 10b, where the RMSE increases with increasing n-factor. However, the numbers remain within the same order of magnitude as the nominal case. Also, these results indicate that the INDI controller is barely affected by aerodynamic uncertainty applied to the aerodynamic coefficients.

IV. Conclusions

After analysing the stability and handling qualities of the Flying-V, it is concluded that the requirements are met the least during approach conditions at the forward centre of gravity location. Therefore, an Incremental Nonlinear

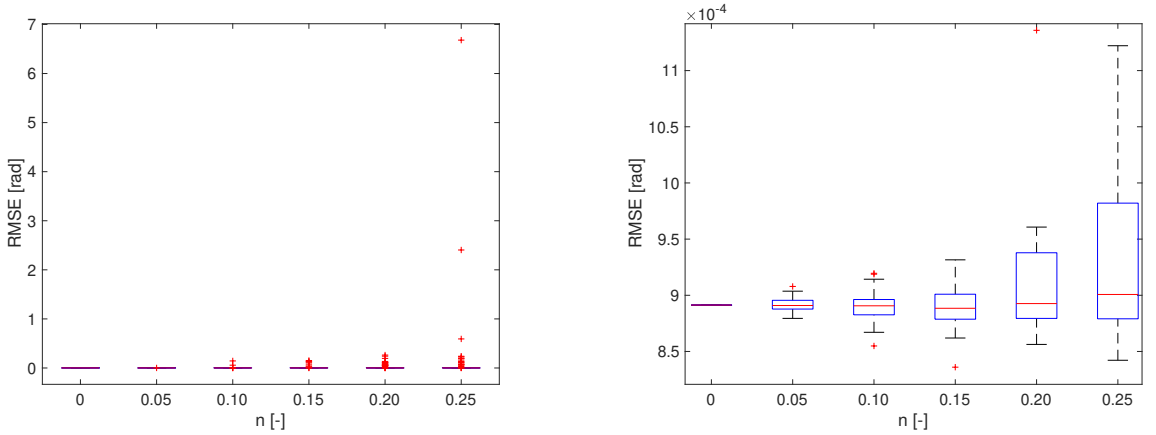

(a) Boxplot for roll angle trajectory.

(b) Zoomed boxplot roll angle.

Fig. 11 Boxplots showing roll angle tracking error for aerodynamic uncertainty.

Dynamic Inversion (INDI) controller is applied to the Flying-V that is able to control the roll angle, flight path angle, and sideslip angle. Using this flight control system the eigenvalues of the Flying-V are located on the left half-plane, indicating that the eigenmodes of the aircraft are stable.

Furthermore, the robustness of the flight control system is assessed by analysing the Root-Mean-Square Error (RMSE) of the Flying-V subjected to aerodynamic uncertainty aiming to follow a 3211 reference trajectory. Even though the flight control system proves to be robust in case aerodynamic uncertainty is applied to the Flying-V. The control surface deflection limits are the only factors limiting the robustness of the flight control system. Namely, excessive control surface deflection demands are required in case the control effectiveness of the control surfaces is decreased. The physical inability of the Flying-V to meet these demands results in an increased RMSE.

Finally, even though previous research indicates that the Flying-V is not able to meet all stability and handling qualities, this research shows that the stability and handling qualities can be improved by designing an INDI controller. Additionally, this controller proves to be robust under the influence of aerodynamic uncertainty. Therefore, this research contributes to the development of the Flying-V by showing that the application of a flight control system is able to improve the stability and handling qualities of the aircraft. Also, due to the robustness of the INDI controller in case of aerodynamic uncertainty, it is possible to start developing a flight control system early in the design phase of the aircraft.

V. Recommendations

With the goal to further improve research on the stability and handling qualities of the Flying-V using an Incremental Nonlinear Dynamic Inversion controller, future work may include the set of items discussed in this section.

During this research, the magnitude of the aerodynamic uncertainty applied to the Flying-V is based on previous research requiring several assumptions to find the maximum aerodynamic uncertainty. It is therefore suggested to perform additional research on the magnitude of the aerodynamic uncertainty to increase the fidelity of the robustness analysis.

Secondly, this research does not analyse the effect of the flight control system on the Control Anticipation Parameter. To perform this analysis, it is necessary to find a lower order equivalent system that translates the pilot input to the pitch rate. For future research, it is therefore suggested to analyse the Control Anticipation Parameter of the controlled Flying-V using a lower order equivalent system.

Besides that, this research only considers aerodynamic uncertainty for the robustness analysis. Therefore, it is suggested to perform additional research on other factors that may affect the stability of the INDI controller such as measurement time delay, sampling frequency, inertia uncertainty, and centre of gravity mismatch.

Furthermore, during this research the outboard elevons and the rudders are used for roll angle control of the Flying-V. Due to the low roll angle that can be achieved without saturating the control surfaces, it is suggested to also incorporate the inboard elevons for roll control in future research.

Finally, this research does not take into account sensor dynamics, nor does it take into account atmospheric effects

such as turbulence. To increase the fidelity of the controller analysis, it is suggested to apply these components to the simulation model.

References

[1] Martinez-Val, R., Perez, E., Puertas, J., and Roa, J., "Optimization of Planform and Cruise Conditions of a Transport Flying Wing," *Proceedings of the Institution of Mechanical Engineers, Part G: Journal of Aerospace Engineering*, Vol. 224, No. 12, 2010, pp. 1243–1251. https://doi.org/10.1243/09544100JAERO812.

[2] Faggiano, F., Vos, R., Baan, M., and Van Dijk, R., "Aerodynamic Design of a Flying V Aircraft," *17th AIAA Aviation Technology, Integration, and Operations Conference*, 2017. https://doi.org/10.2514/6.2017-3589.

[3] Martinez-Val, R., "Flying Wings: A New Paradigm for Civil Aviation?" *Acta Polytechnica Vol. 47 No. 1/2007*, 2007. https://doi.org/10.14311/914.

[4] Okonkwo, P., and Smith, H., "Review of Evolving Trends in Blended Wing Body Aircraft Design," *Progress in Aerospace Sciences*, Vol. 82, 2016, pp. 1–23. https://doi.org/10.1016/j.paerosci.2015.12.002.

[5] Zhenli, C., Zhang, M., Yingchun, C., Weimin, S., Zhaoguang, T., Dong, L., and Zhang, B., "Assessment on Critical Technologies for Conceptual Design of Blended-Wing-Body Civil Aircraft," *Chinese Journal of Aeronautics*, Vol. 32, No. 8, 2019, pp. 1797–1827. https://doi.org/10.1016/j.cja.2019.06.006.

[6] Liebeck, R. H., "Design of the blended wing body subsonic transport," *Journal of aircraft*, Vol. 41, No. 1, 2004, pp. 10–25. https://doi.org/10.2514/1.9084.

[7] Benad, J., "The Flying V, A New Aircraft Configuration for Commercial Passenger Transport," *Deutscher Luft- und Raumfahrtkongress*, 2015. https://doi.org/10.25967/370094.

[8] van Overeem, S., Wang, X., and Van Kampen, E.-J., "Modelling and Handling Quality Assessment of the Flying-V Aircraft," *AIAA SCITECH 2022 Forum*, 2022, p. 1429. https://doi.org/10.2514/6.2022-1429.

[9] Cappuyns, T., "Handling Qualities of a Flying V Configuration," http://resolver.tudelft.nl/uuid:69b56494-0731-487a-8e57-cec397452002, 2019.

[10] Garcia, A.R., "Aerodynamic Model Identification of the Flying V using Wind Tunnel Data," http://resolver.tudelft.nl/uuid:79e01f29-1789-4501-8556-ca2bcf06f3ab, 2019.

[11] Palermo, M., and Vos, R., "Experimental Aerodynamic Analysis of a 4.6%-Scale Flying-V Subsonic Transport," *AIAA Scitech 2020 Forum*, 2020, p. 2228. https://doi.org/10.2514/6.2020-2228.

[12] Balas, G.J., "Flight Control Law Design: An Industry Perspective," *European Journal of Control*, Vol. 9, No. 2-3, 2003, pp. 207–226.

[13] Slotine, J.E. et al., *Applied Nonlinear Control*, Vol. 199, Prentice hall Englewood Cliffs, NJ, 1991.

[14] Adams, R.J. et al., "Robust Flight Control Design using Dynamic Inversion and Structured Singular Value Synthesis," *IEEE Transactions on control systems technology*, Vol. 1, No. 2, 1993, pp. 80–92.

[15] Wang, X., Van Kampen, E.-J., Chu, Q., and Lu, P., "Stability analysis for incremental nonlinear dynamic inversion control," *Journal of Guidance, Control, and Dynamics*, Vol. 42, No. 5, 2019, pp. 1116–1129. https://doi.org/10.2514/1.G003791.

[16] Wang, X., and Van Kampen, E.-J., "Incremental backstepping sliding mode fault-tolerant flight control," *AIAA Scitech 2019 Forum*, 2019, p. 0110. https://doi.org/10.2514/6.2019-0110.

[17] Wang, X., Kampen, E.-J. v., Chu, Q., and Lu, P., "Incremental sliding-mode fault-tolerant flight control," *Journal of guidance, control, and dynamics*, Vol. 42, No. 2, 2019, pp. 244–259. https://doi.org/10.2514/1.G003497.

[18] Viet, R., "Analysis of the Flight Characteristics of a Highly Swept Cranked Flying Wing by Means of an Experimental Test," http://resolver.tudelft.nl/uuid:90de4d9e-70ae-4efc-bd0a-7426a0a669c3, 2019.

[19] Anonymous, "Military Specifications, Flying Qualities of Piloted Aircraft MIL-F-8785C," , 1980.

[20] Cook, M.V., *Flight Dynamics Principles: A Linear Systems Approach to Aircraft Stability and Control*, Butterworth-Heinemann, 2012.

[21] Sieberling, S et al., "Robust Flight Control using Incremental Nonlinear Dynamic Inversion and Angular Acceleration Prediction," *Journal of Guidance, Control, and Dynamics*, Vol. 33, No. 6, 2010, pp. 1732–1742.

[22] Acquatella, P. et al., "Robust Nonlinear Spacecraft Attitude Control using Incremental Nonlinear Dynamic Inversion," *AIAA Guidance, Navigation, and Control Conference*, 2012, p. 4623.

[23] Matamoros, I., and de Visser, C. C., "Incremental Nonlinear Control Allocation for a Tailless Aircraft with Innovative control Effectors," *2018 AIAA Guidance, Navigation, and Control Conference*, 2018, p. 1116.

[24] Tang, S.H., "Fault-Tolerant Flight Control with Sensor-Based Nonlinear Dynamic Inversion: Application and Evaluation in the SIMONA Research Simulator," http://resolver.tudelft.nl/uuid:c2263beb-602b-4727-9219-43cd11325622, 2014.

[25] European Union Aviation Safety Agency, "Type-Certificate Data Sheet No. E.111 for Trent XWB Series Engines," 2019, p. 7.

[26] Ridcully, M., "A350-900: Flight Deck and Systems Briefing for Pilots," , 2011.

[27] Van 't Veld, R. C., Van Kampen, E., and Chu, Q. P., "Incremental Nonlinear Dynamic Inversion Flight Control: Stability and Robustness Analysis and Improvements," *AIAA Aircraft Flight Control Design Conference*, 2018. https://doi.org/10.2514/6.2018-1127.